IIUC Journal of Science and Engineering
Vol.-2, Issue-1, December 2024, pp. 185-208
ISSN: 3005-5873

Analysis of labyrinth-maze-shaped metamaterial for efficient airplane altimeter applications

Saif Hannan
Department of Electronic and Telecommunication Engineering
International Islamic University Chittagong (IIUC), Bangladesh

Article info

Keywords
Absorber
Altimeter
Metamaterial
Polarization-insensitive
5G

Abstract

This paper proposes an analytical description of a unique labyrinth-maze-shaped metamaterial for electromagnetic noise reduction applications in airplane communications systems. The proposed metamaterial has shown a single negative value and negligible reflection coefficient near 5 GHz for FR4 as a dielectric spacer with any thickness. In airplanes, many antennas and radars are used at different frequencies, which sometimes may interfere with other frequencies transmitted from the ground. The proposed metamaterial can eliminate such EM interference at frequencies near 5 GHz. Moreover, the metamaterial has shown incident angle insensitivity up to 180 degrees phi and 80 degrees theta along with TE and TM mode of EM wave. With a solid copper ground, it can act as an absorber with absorptions at 4.12 GHz and 5.248 GHz, which may isolate the altimeter radar system of the airplane from external mid-band 5G frequencies and thus ensure smooth functioning of both the 5G mobile and the airplane altimeter communications systems.

Corresponding author
Saif Hannan
Department of Electronic and Telecommunication Engineering, International Islamic University Chittagong, Kumira, Chattogram, Bangladesh - 4318
Email: sh@iiuc.ac.bd

Introduction

A metamaterial is an artificially designed structure or scientific object that exhibits some electromagnetic properties that we usually can't anticipate from an artificially or naturally generated substance. To achieve the primary property of the metamaterial, the refractive index must be made negative (Landy, Sajuyigbe, Mock, Smith, & Padilla, 2008). To attain that, it is essential for the real part of either permittivity or permeability, or both, to be close to zero or negative, and it is also necessary for the

imaginary parts to be close to zero. There is a potential of attaining a negative value of permittivity or permeability when the values of the reflection coefficient and transmission coefficient trace from opposite sides and just touch or look like they are touching one another. This occurs when the values of the reflection coefficient and transmission coefficient originate from opposite sides (Uddin, Hannan, Hossen, Gafur, Rashid, Uddin, & Chowdhury, 2023).

Antenna gain enhancement, stealth applications, crowd sensing, radar cross-section reduction, electromagnetic energy harvesting, specific absorption rate reduction, coupling reduction from 5G or MIMO antenna systems, and other relevant applications depend on appropriate metamaterials, and it is increasing at the present time. Several distinct kinds of materials have been tried and tested for use in constructing microwave metamaterial absorbers. Copper, tungsten, graphene, and silicon dioxide, as well as FR-4 and other materials, are among the most often utilized components as dielectric spacer between the patch and the ground (Ramachandran, Faruque, Siddiky, & Islam, 2021). Copper was used throughout the design process for both the patch and the ground, while FR-4 was chosen as the substrate. Even though it has a significant dielectric loss, the material that we selected to design the substrate is not challenging to locate and has a reasonable cost of production (Haque, Hossain, Ahmed, & Namihira, 2018; Afsar, Faruque, Hossain, & Islam, 2023).

This paper presents an 8mm width and length-based metamaterial absorber with a unique Labyrinth-Maze-Shaped patch on an FR4 substrate for use in aviation communication applications. It will be operated in the C band frequency region, where metamaterial features will also be present, boosting the absorber's usefulness by increasing the range of frequencies it can absorb.

CST 2017 was utilized throughout the simulation process for designing the absorber, and the simulation took about ten to twelve minutes on average.

Basics of metamaterial properties

The metamaterial properties of an absorber depend on the structure of the patch, ground, and substrate. At present, no method is available to find metamaterial properties. In addition, to get metamaterial properties, the first condition is to get absorption, where the reflection and transmission coefficients must be under -10dB. To find the absorption, we have to subtract the reflection and transmission coefficients from the supplied electromagnetic energy (Ushikoshi et.al., 2023).

$$Absorption(A) = 1 - |\text{ Reflection Coefficient }|^2 - |\text{ Transmission Coefficient }|^2 \quad (1)$$

Here, the reflection coefficient can be defined as $S_{11,}$ and the transmission coefficient as S_{21}. There is a possibility that absorption is only dependent on the reflection coefficient if a solid metal ground is used. Electromagnetic waves cannot intersect the metallic surface; thus, the value of S_{21} will become zero, and the absorption will be,

$$Absorption(A) = 1 - |\text{ Reflection Coefficient }|^2 \quad (2)$$

The next aim will be to get the permittivity and permeability in the range where they can fulfill the condition for the structure to be metamaterial. For that, one of the real part values of permittivity or permeability needs to be near zero or negative; conversely, the imaginary parts also need to be near zero to call it a single negative (SNG) value. If both the epsilon and mu values follow this condition, there will be a double negative value. In this way, both SNG and DNG metamaterial properties can be found (Hannan, Islam, Faruque, Chowdhury, & Musharavati, 2021).

$$S11(\omega) = \frac{Z(\omega) - Zo}{Z(\omega) + Zo} \quad (3)$$

Z (ω) is the impedance of the absorber, whereas Z_0 is the free space impedance (377 ohms). EM wave fall onto the surface of the absorber, the loss of energy happens because of reflection and absorption can be calculated by the following equations (Norouzi et.al., 2023),

$$Loss_R = 10\ log\left(\frac{1}{1 - S11^2}\right) = -10\ log(1 - R) \quad (4)$$

Here, R represents the reflection coefficient S_{11}, where LOSSR represents the reflection loss of the absorber. Absorption loss can be found by,

$$Loss_A = 10\ log\left(\frac{1 - S11^2}{S21^2}\right) = -10\ log\left(\frac{T}{1 - R}\right) \quad (5)$$

In the above equation, T denotes the transmission coefficient S_{21}. Division of the impedance subtraction and addition provide the value of the reflection coefficient. Impedance in both the absorber and free space depends on permeability and permittivity (Capolino, 2017a; Capolino, 2017b).

$$Z(\omega) = \sqrt{\frac{\mu_0(\omega)\mu_f(\omega)}{\varepsilon_0(\omega)\varepsilon_f(\omega)}} \quad (6)$$

Here, the $\mu_0(\omega)$ and $\varepsilon_0(\omega)$ are the permeability and permittivity applicable to both the absorber and free space, which we must evaluate to obtain the absorber's impedance.

$$Z_0 = \sqrt{\frac{\mu_0(\omega)}{\varepsilon_0(\omega)}} \quad (7)$$

The free space impedance depends only on free space permittivity (ε_0) and permeability (μ_0), and the value is generally 377ohm.

Design of the metamaterial unit cell

The design of the unit cell began with the shape of a labyrinth or maze on the patch structure. This structure was chosen by inspiration from the Greek mythology. A central square path is surrounded by two structures that are shaped similarly and have continuous paths leading to the center that are connected to each other. As seen in Figure 1(a), the forms have their opposite sides facing outward to produce a path that resembles a maze leading toward the center of the structure. Ground is the name given to the copper surface that serves as a support for the rear side of the unit cell (Elakkiya, Mohanan, Thomas, & Ahmedh, 2023). The initial decision for the dielectric spacer was to go with FR4 because of its dielectric constant of 4.3 and its thickness of 1.6 millimeters. Because of the dielectric spacer, the two continuous routes have the potential to produce resonance frequency as well as inductive and capacitive loads (Ioannides, 1998). The particular dimension of the patch structure is depicted in further detail in figure 1(b)(Hannan, Islam, Almalki, Faruque, & Islam, 2022).

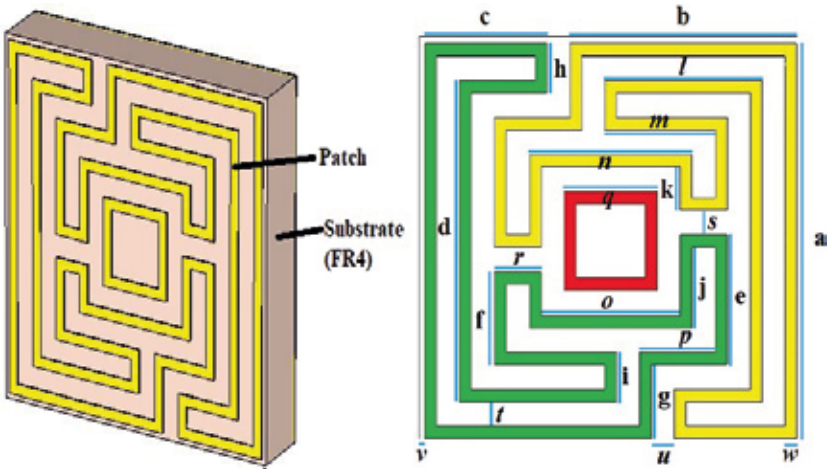

Figure 1
Structure of the (a) unit cell and (b) patch with detailed dimensions

Table I
Detailed dimension of the patch on the unit cell

a = 8 mm	b = 4.875 mm	c = 2.625 mm	d = 6.5 mm	e = 2.625 mm
f = 1.875 mm	g = 1.5 mm	h = 1 mm	i = 1 mm	j = 1.625 mm
k = 1.375 mm	l = 3.375 mm	m = 2.375 mm	n = 3.5 mm	o = 3 mm
p = 1.625 mm	q = 2 mm	r = 1 mm	s = 0.5 mm	t = 0.5 mm
u = 0.5 mm	v = 0.125 mm	w = 0.25 mm		

The patch and the ground were focused on the EM wave port, with port 1 facing the patch and port 2 facing the ground. It is essential to mention that the patch is not composed of a single piece of flat, solid metal, whereas the ground is formed of a single piece of fully conductive metal. There is a coefficient for the amount of EM wave that is reflected, but there is no coefficient for the amount of wave that is transmitted due to solid ground (Hannan, Islam, Soliman, Sahar, Singh, Faruque, & Alzamil, 2022).

Simulation methods

The simulation was performed on commercially available CST Microwave Studio Suite software with the detailed dimension of the patch shown in Figure 1 and Table I. The patch and the solid ground were chosen with annealed copper from the component library in CST with 0.035 mm thickness, and a dielectric spacer of 1.6mm thickness (FR4 with dielectric constant of 4.3) was set between the patch and the ground. The proposed design (metamaterial absorber) was placed along the x-y plane, and an electromagnetic wave was applied along the z-axis. The operating frequency was set from 4 to 6 GHz to get EM absorptions, probably at frequencies for 5G mobile and airplane altimeter communications systems. S parameters were extracted from CST after simulation to calculate the desired performance of the absorber, as discussed in the next section.

Analysis of the metamaterial

When the electric field is discussed for a metamaterial absorber, the amount of attraction or repulsion experienced by an outside charge when it enters the field of another charge is because both charges interact with each other. An electric and magnetic (EM) force is produced as a result of the motion of the electric charge. The electric and the magnetic field radiation are depicted for understanding in Figs. 2 and 3, respectively. The surface current that is produced is due to the energy from the EM wave that meets the surface of the absorber. The electromagnetic radiation did not affect any part of the surface, and there was a coupling between the surface currents generated under the patch and the ground. In other

words, into the substrate that is sandwiched between the patch and the ground, where depending on the frequency, the energy is absorbed after being agitated on the surface (Chowdhury, Islam, Hossain, Alsaif, Alshammari, Alzamil, & Samsuzzaman, 2023). When it comes to carrying out the method correctly, flux density is one of the most important factors to consider. The rule states that the larger the applied electric field, the bigger the electric flux density. The region denoted by red is the portion of the substrate's surface that experiences the most significant amount of surface current generation. The greater the freedom of movement of current, the greater the resonance, and the gap between the inductive material and the capacitive gap is where the ability to control the intended frequency. Another aspect to consider is that the maximum absorber has a design incorporating numerous layers of substrate and ground, making the overall construction more difficult and expensive. Additionally, the utilization of this material lends the absorber a degree of flexibility, which is beneficial to the use case of the absorber in several specific domains (Kim, Jung, Choi, Hwang, & Hyun, 2022; Panwar, & Lee, 2017). The intensity of an absorber's surface current, expressed as a value per square meter of the absorber's surface area, is shown on the scale in Figure 4.

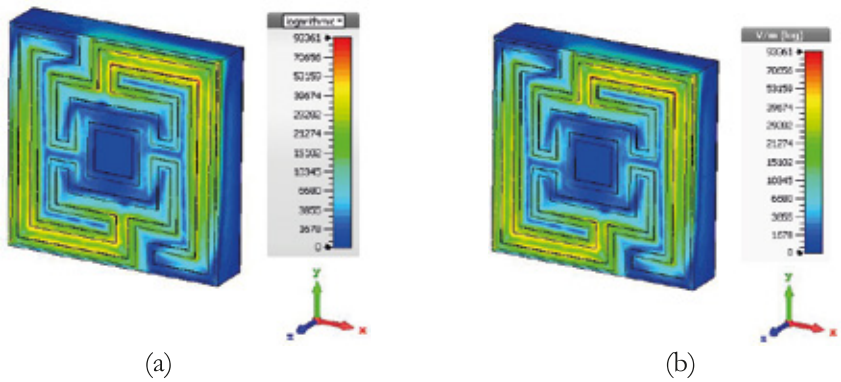

Figure 2
Electric field distribution at (a) 4.12 GHz and (b) 5.248 GHz

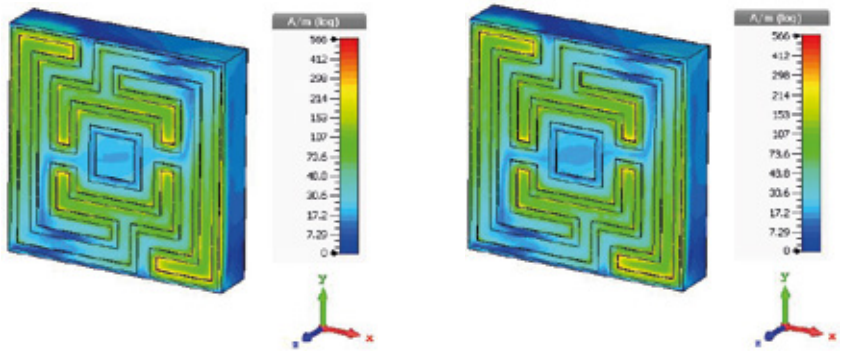

Figure 3
Magnetic field distribution at (a) 4.12 GHz and (b) 5.248 GHz

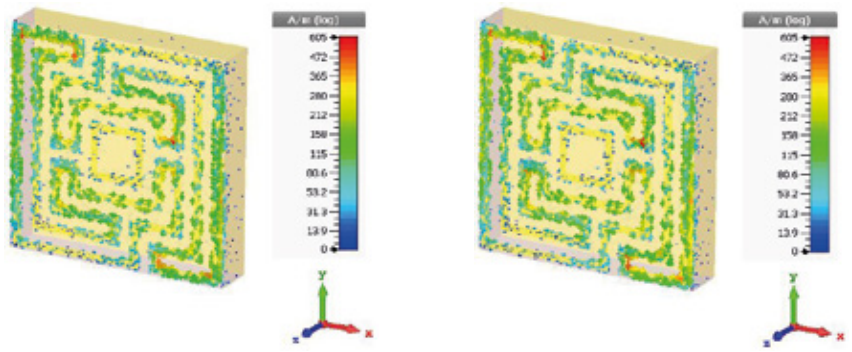

Figure 4
Surface current distribution at (a) 4.12 GHz and (b) 5.248 GHz

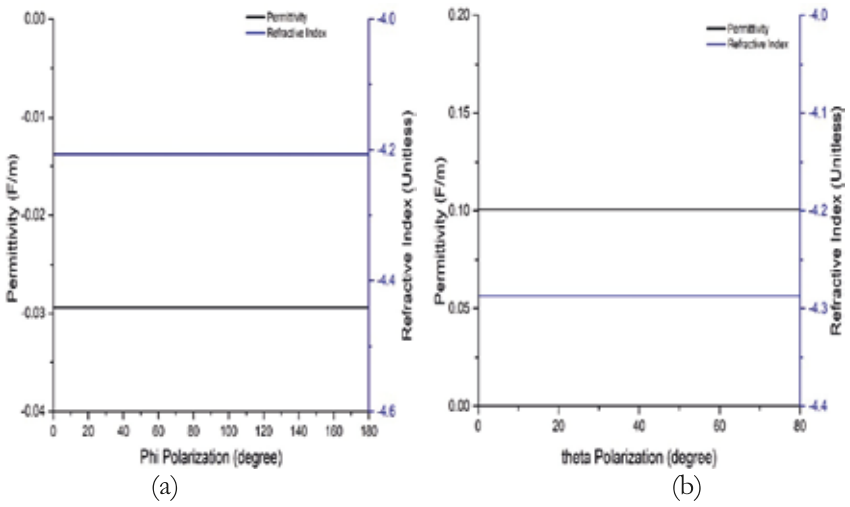

Figure 5
Change of permittivity and refractive index with (a) Phi and (b) Theta

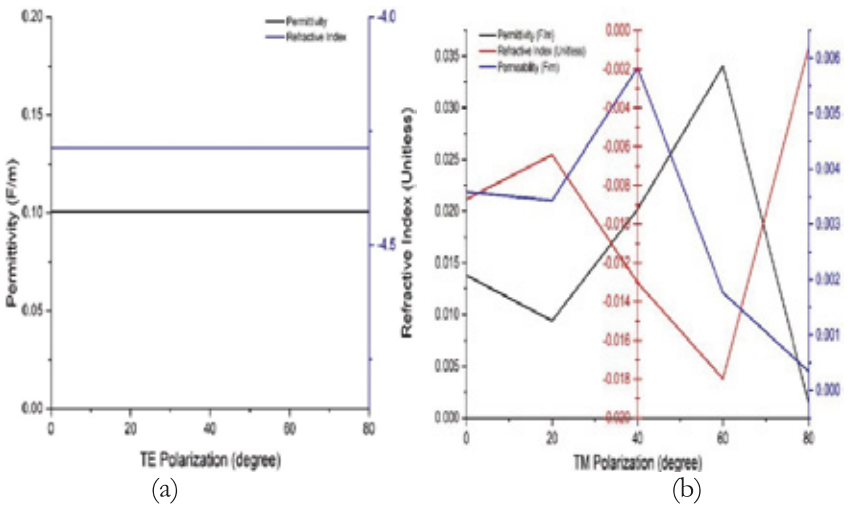

Figure 6
Permittivity and refractive index for (a) Transverse electric and (b) Transverse magnetic mode

When the magnetic shielding for the electric field and electric shielding for the magnetic field are applied, a clear view of the transverse electric (TE) and transverse magnetic (TM) fields are achieved and depicted, as shown in Figure 6.

There are cases when the behaviour of the absorber remains the same for each field, and sometimes some differences are observed. Compared

to the TE and TM modes, the results of the permittivity and refractive index values show some differences between the two. These differences are shown in Fig. 6 (Saadeldin, Sayed, Amr, Sayed, Hameed, & Obayya, 2023). Nevertheless, broad-angle absorptions with metamaterial properties (Schultz, 2023; Zolfaghary pour, Chegini, & Mighani, 2023) were successfully obtained, which cannot be seen in other recent papers with sufficient evidence.

Data for FR4

A minimum of -10 dB value S parameters for absorption were considered when the resonances occurred at 4.12 GHz and 5.248 GHz. This gave the maximum amount of absorbed energy. Permittivity and permeability exhibited near-zero values in this frequency range but not at the same frequencies as the observed absorptions. These values can be found between these frequencies. This phenomenon of getting metamaterial properties at other frequencies where absorptions are not maximum is accepted by the scientific community (Hossain, Faruque, & Islam 2023).

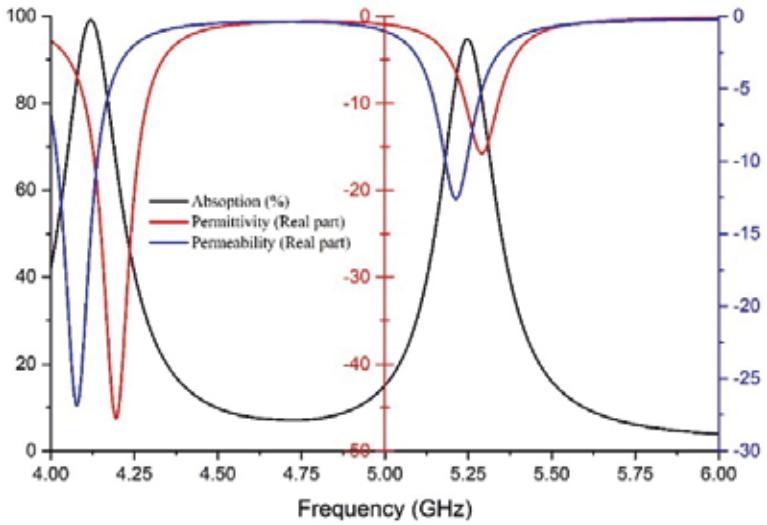

Figure 7

Absorption, permittivity, and permeability for FR-4 substrate

During the design process with FR-4, how the material influences the metamaterial absorber's capacity to take into account was monitored. For the designed absorber, the results obtained with various substrate materials were essential to demonstrate that the outcomes obtained from using a FR-4 substrate and other materials were stable. FR-4 gave the best results for the absorber due to its high dielectric constant (Kim, 2023;

Hafidzurrahman, Yudistira, Riayatsyah, & Saputro, 2023). There are three distinct possibilities: one involves using the entire ground, another involves utilizing some part of the ground, and the third possibility involves using none of the metal ground. It was observed that the results of using either a complete or partial copper ground gave the most number of absorption peaks. In contrast, the results of utilizing no ground gave only the absorption at a single frequency (Yufei, Wenrong, Xiaonan, & Guoqiang, 2023). The information that may be gleaned from Figure 8.

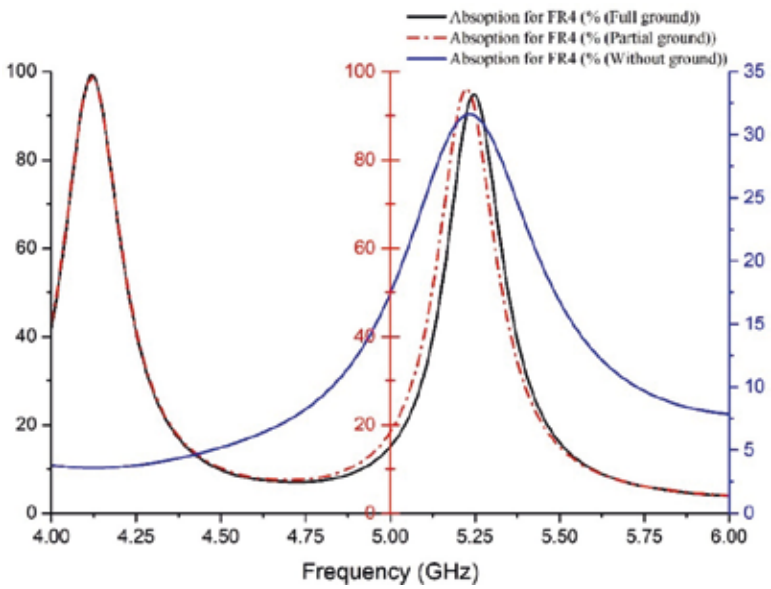

Figure 8
Absorption for different scenarios

The same three scenarios were found in the case of permittivity, and a value close to zero in 4.172 GHz was achieved when either a complete or partial ground was considered. However, if near zero permittivity was not found, it couldn't exhibit any metamaterial properties at any frequencies (Hannan, Islam, Faruque, & Rmili, 2021) where resonance peaks might be found.

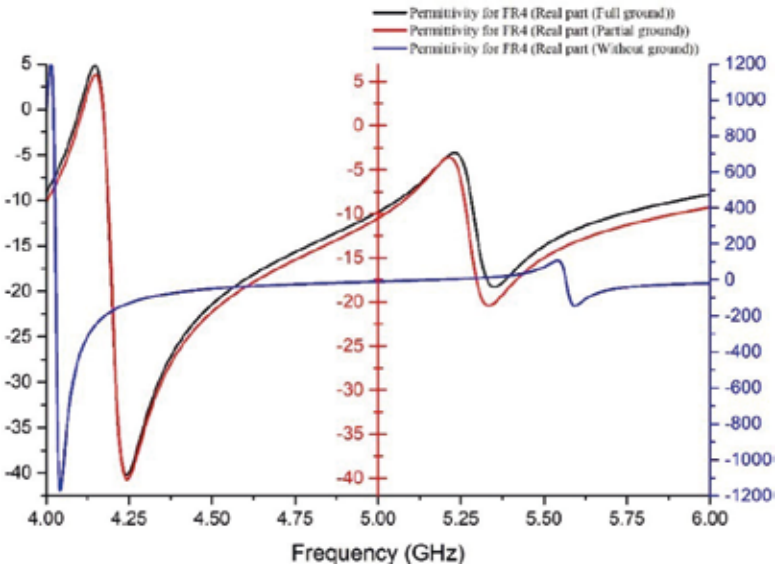

Figure 9
Permittivity for different scenarios

Since solid ground was considered at different angles of phi and theta, groundless absorbers were useless when comparing the findings. On the graph, each scale is adjusted so that it can be measured from a different perspective. The colour black on the scale was used to measure the results for total ground, while the red and blue represent observations of permittivity for the partial ground and no ground results, respectively, as shown in Figure 10.

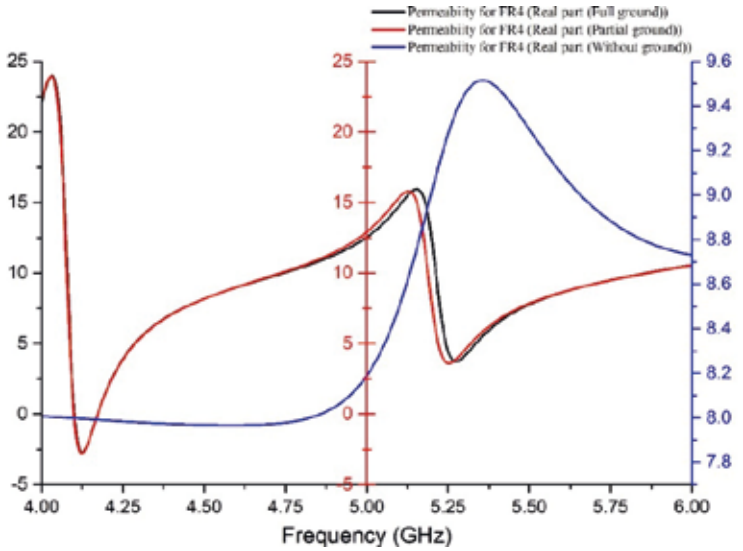

Figure 10
Permeability for different scenarios

In Figures 8 to 10, the use of complete and partial ground is depicted, and it was necessary to analyze the metamaterial properties at different conditions (Moniruzzaman, Islam, Mansor, Soliman, Misran, & Samsuzzaman, 2023) to reach the best decision for taking ground either as complete ground or partial ground.

With ground

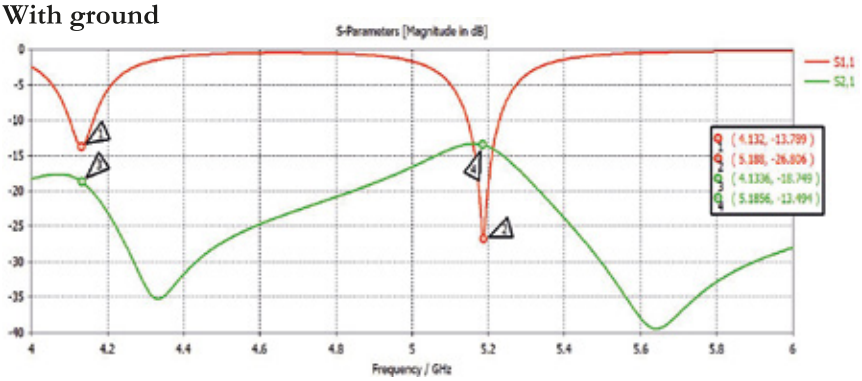

Figure 11
Reflection and transmission Coefficient with ground

When ground was used, a more significant amount of inductive material was involved, which changed the absorber's outcome. Since electromagnetic (EM) waves cannot intersect the ground completely, this

will lead to an increase in the amount of energy absorbed. This is demonstrated clearly in Fig. 11 as reflection and transmission coefficients for better consideration (Berka, Özkaya, Islam, El Ghzaoui, Varakumari, Das, & Mahdjoub, 2023).

Without ground

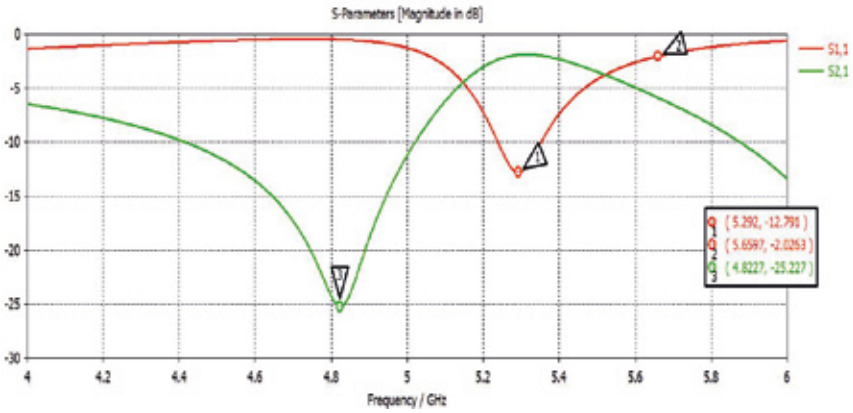

Figure 12
Reflection and transmission Coefficient without ground

There are no obstructions for transmission when the absorber is acting without ground. A dielectric substrate is employed in the absorber and is responsible for transmission management (Sakib et. al., 2023). Since most of the electromagnetic waves penetrated the surface of the patch, the signal was sent to the other side because there was no ground on that side.

Simplified equivalent circuit

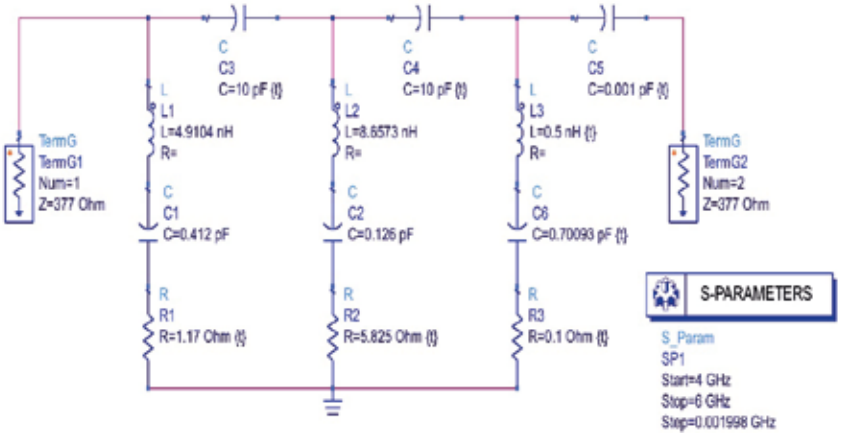

Figure 13
Equivalent circuit of the proposed absorber

The same conclusion can be obtained using an ADS circuit simulation, in which L and C are calculated following the surface current inductive portion for a specific frequency at which resonance occurs. In this case, two RLC circuits (L1, C1, R1, L2, C2, R2) are functioning, and to make a capacitive gap work for the substrate between the ground and the waveguide port of the EM source, another RLC circuit (L3, C6, R3) has been included. Both of these resonance frequencies are accommodated by the two RLC circuits (Fig. 13). Since the patch does not consist entirely of metal, the space that exists in between each patch has the electrical properties of a capacitor (C3, C4 and C5). In this case, the impedance in both ports is 377 ohms, corresponding to free space (Hannan, Islam, Sahar, Mat, Chowdhury, & Rmili, 2020).

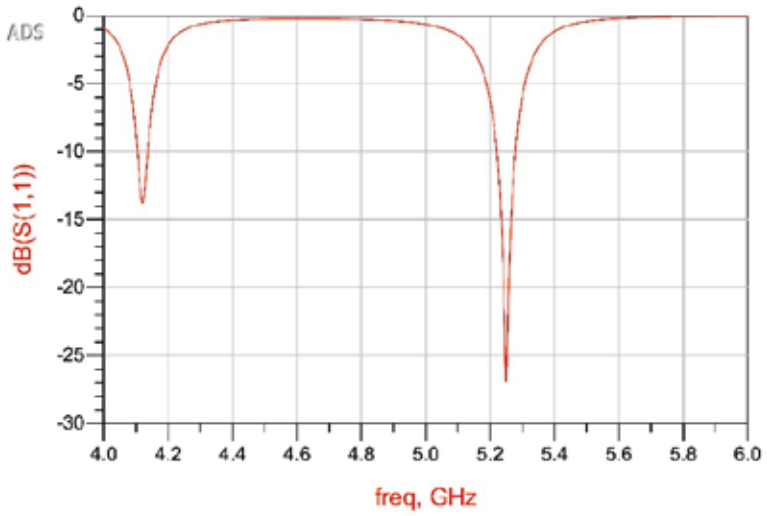

Figure 14
Reflection coefficient according to the ADS circuit simulation

The result seen in Fig. 14 comes from a simulation of an ADS circuit, and it is essentially identical to the result that was received from the CST simulation in Fig. 12. While electromagnetic (EM) waves strike the surface of the unit cell, the energy that is transferred into the unit cell activated the characteristics of inductive and capacitive properties. These are the features that were taken into consideration while designing the ADS circuit. Both inductive and capacitive portions contribute to the process of finding the resonance that is below -10 dB and also change the resonance (Hannan, Islam, Almutairi, &Faruque, 2020b).

Data for array

After the array was simulated in CST, the necessary dxf file was extracted to allow the absorber to be fabricated. A 6 × 3 array absorber has been simulated and manufactured, and it can be observed that the surrounding absorber coupling does not cause any change in the outcome of the absorber. This indicates that the absorber can serve as a possible absorber for a particular application. It is clear that there is some space between the absorbers; nevertheless, given that the entire ground was employed, the ground array section as a whole does not contain any spaces (Ra'di, Simovski, & Tretyakov, 2015; Pang et.al., 2021).

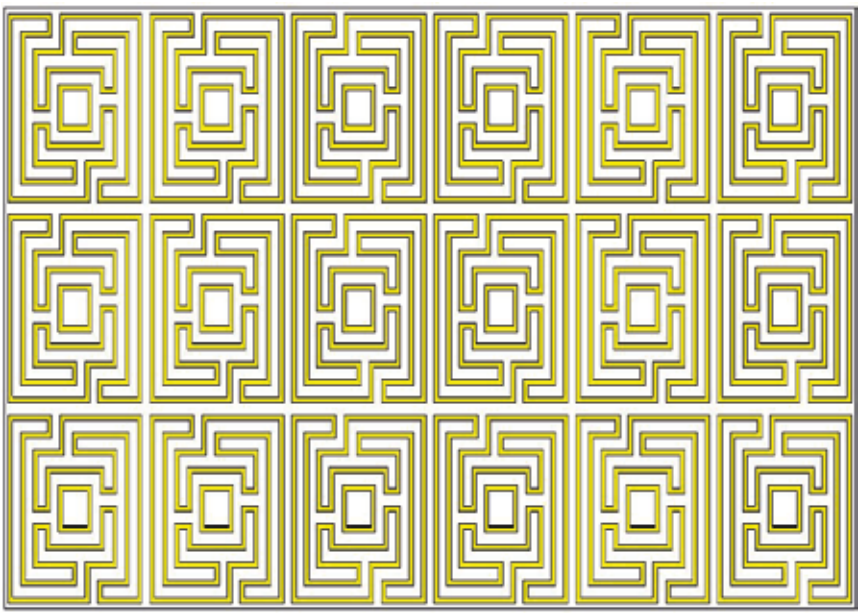

Figure 15
Array in CST

Experimental validation

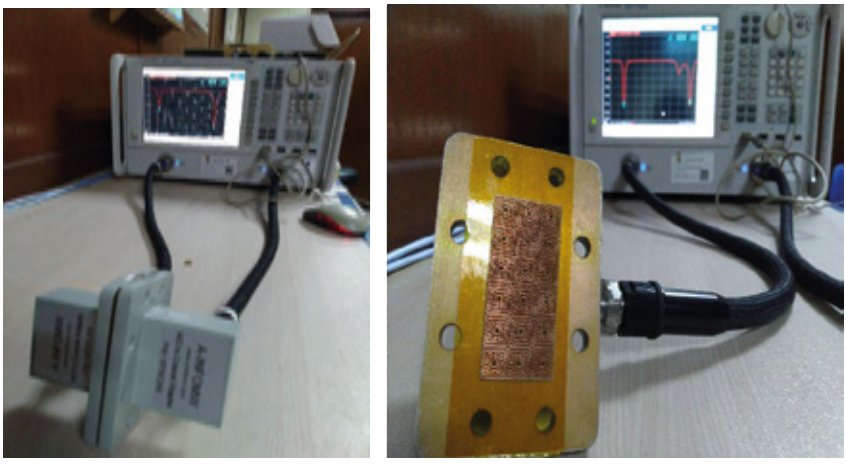

Figure 16
Experimental validation with Vector Network Analyzer (VNA) report

After fabrication, the results found from the CST simulation were compared with the VNA result and checked whether the absorber showing absorption was practically correct. Sometimes, resonance frequency shifts a bit forward or backward because of coupling with the surroundings of the absorber (Hasan, Faruque, & Islam, 2018). Here, no change in absorption results was noticed because of coupling. VNA is connected to a waveguide port and sends EM waves through the absorber. VNA then tests the result across its terminal (Kapoor, Mishra, & Kumar, 2022) in Fig. 16, the waveguide to the coaxial adapter comes from VNA, and between them, a unit cell or array is connected, from which absorption was obtained.

Discussion

The absorber was proved insensitive to co-polarization and cross-polarization of the incident EM waves, and this proposed wide-incident angle insensitive absorber has a few potential applications that were possible due to its characteristics (Chowdhury, Hannan, Uddin, Bhuiyan, Hoque, & Islam, 2023). The larger the absorber, the greater its efficiency, and the more it contributes to meeting the requirements of the subwavelength condition. It is necessary to provide a comparison of the similar works done by others in recent times to raise awareness about the potential the proposed absorber has for helping people, as shown in table II. From the comparison table, it can be observed that the application of

maximal absorbers did not have any specific applications. This is because the size and EMR ratio are not impactful enough to decrease the operating field (Jahan, Faruque, & Hossain, 2023; Patel, Parmar, & Katkar, 2022).

Table II
Comparison with recent similar works

Article	Size (mm)	Resonance (GHz)	Angle Insensitivity (⁰)	SNG / DNG	Absorption (%)	EMR (λ/L)	Application
Hossain et.al, 2022	0.118λ × 0.118λ	3.94, 8.08, and 11.17GHz	Till 60	SNG	Not Mentioned	8.5	S, C, and X bands satellite & radar communication
Bennaoum, Berka, Bendaoudi, Rouabhi, & Mahdjoub, 2023	0.385λ × 0.385 λ	6.43, 9.10, 11.86 and 14.67 GHz	Not Mentioned	Not Mentioned	89.40, 99.66, 99.10, and 95.22%	5.8	Sensors and RADAR systems
Deng et al., 2020	0.226λ × 0.226 λ	8.5, 13.5, and 17 GHz	Up to 60	Not Mentioned	99.9%, 99.5%, and 99.9%	4.4	at X and Ku Frequency Band
Sakib et. al., 2023	0.096λ × 0.096 λ	1.44, 3.96, 4.205, and 5.025 GHz	75	SNG	99.382%, 99.383%, 99.91%, and 95.17%	10.4	S-band
Presented	0.12λ × 0.12λ	4.12GHz, and 5.248GHz	80	SNG	99.98%, 98.2%	9.1	Airplane Communication

The absorber under consideration has a favourable EMR (effective medium ratio) that qualifies it as a potential candidate for using in appropriate communication devices as sensors. In addition, it is designed to perform some functions, and the fact that it may be used in conjunction with a wide variety of other metamaterials demonstrates the importance of the paper in this context. When comparing the outcomes of the absorber, different types of substrate material (plexiglass, rubber, and FR-4) were utilized (Lee, Hwang, Lim, Hara, & Lim, 2016). Applications for the C and X bands can be found on antennas, fighter aircraft systems, and satellites at 4.12 and 5.248 GHz, respectively. A satellite's C-band downlink frequency can be set to 4.12 GHz, and its uplink frequency can be set to 5.248 GHz (ITU, 2019; Hannan, Islam, Faruque, Chowdhury, & Musharavati, 2021).

Conclusion

An absorber of dimension 0.12λ × 0.12λ with a unique labyrinth-maze-shaped patch structure was developed as a unit cell and array on FR4 substrate. Two resonance frequencies at 4.12 GHz and 5.248 GHz were achieved with a maximum of 99.8% absorptions that fall in the applications of aircraft altimeter navigation frequency. The absorber was fabricated and validated with a vector network analyzer (VNA) to compare the performance as per simulation results for both the unit cell and array. In airplanes, many antennas and radars are used at different frequencies, which sometimes may interfere with other frequencies transmitted from the ground. The proposed metamaterial can eliminate such EM interference at frequencies near 5 GHz. Moreover, the metamaterial has shown incident angle insensitivity up to 180 degrees phi and 80 degrees theta along with TE and TM mode of EM wave. With a solid copper ground, it can act as an absorber with absorptions at 4.12 GHz and 5.248 GHz, which may isolate the altimeter radar system of the airplane from external mid-band 5G frequencies and thus ensure smooth functioning of both the 5G mobile and the airplane altimeter communications systems.

Acknowledgements

The author did not receive any internal or external funding for this research.

References

Afsar, M. S. U., Faruque, M. R. I., Hossain, M. B., & Islam, M. T. (2023). SRR inspired modified psi shaped perfect metamaterial absorber for C-band application. *Journal of Magnetism and Magnetic Materials*, *582*, 171010.

Bennaoum, M., Berka, M., Bendaoudi, A., Rouabhi, A. Y., & Mahdjoub, Z. (2023). Investigation of a near-perfect quad-band polarization-insensitive metamaterial absorber based on dual-T circular shaped resonator array designed on a silicon substrate for C-, X-and Ku-bands applications. *Silicon*, *15*(2), 699-712. doi: 10.1007/s12633-022-02038-2.

Berka, M., Özkaya, U., Islam, T., El Ghzaoui, M., Varakumari, S., Das, S., & Mahdjoub, Z. (2023). A miniaturized folded square split ring resonator cell based dual band polarization insensitive metamaterial absorber for C-and Ku-band applications. *Optical and Quantum Electronics*, *55*(8), 699. doi: 10.1007/s11082-023-04954-y.

Capolino, F. (2017a). *Theory and phenomena of metamaterials*. Florida, USA: CRC press.

Capolino, F. (2017b). *Applications of metamaterials*. Florida, USA: CRC press.

Chowdhury, A. R., Hannan, S., Uddin, M. K., Bhuiyan, M. E. H., Hoque, M. I., & Islam, M. T. (2023, June). *Gas stove burner shape with inductive tailed rotational symmetric metamaterial absorber for C and X band application*. Paper presented at the 2023 International Conference on Next-Generation Computing, IoT and Machine Learning (NCIM) , Gazipur, Bangladesh (pp. 1-5). IEEE. doi: 10.1109/NCIM59001.2023.10212988.

Chowdhury, M. Z. B., Islam, M. T., Hossain, I., Alsaif, H., Alshammari, A. S., Alzamil, A., & Samsuzzaman, M. (2023). A bendable wide oblique incident angle stable polarization insensitive metamaterials absorber for visible optical wavelength applications. *Optik*, vol. *286*, 171016. doi: https://doi.org/10.1016/j.ijleo.2023.171016.

Deng, G., Lv, K., Sun, H., Yang, J., Yin, Z., Li, Y., ... Li, X. (2020). An ultrathin, triple-band metamaterial absorber with wide-incident-angle stability for conformal applications at X and Ku frequency band. *Nanoscale Research Letters*, *15*, 1-10. doi: 10.1186/s11671-020-03448-0.

Elakkiya, A., Mohanan, A., Thomas, M. A., & Ahmedh, R. S. R. (2023). 6 Bands microwave metamaterial absorber for S, C, X, and Ku band applications. *Materials Today: Proceedings*.

Hafidzurrahman, M., Yudistira, H. T., Riayatsyah, T. M. I., & Saputro, A. G. (2023). Tailoring the refractive index of single layer touching circular metamaterial by adjusting the dielectric thickness. *Materials Letters*, vol.*349*, 134726. doi: https://doi.org/10.1016/j.matlet.2023.134726.

Hannan, S., Islam, M. T., Sahar, N. M., Mat, K., Chowdhury, M. E., & Rmili, H. (2020). Modified-segmented split-ring based polarization and angle-insensitive multi-band metamaterial absorber for X, Ku and K band applications. *IEEE Access*, *8*, 144051-144063. doi: 10.1109/ACCESS.2020.3013011.

Hannan, S., Islam, M. T., Almutairi, A. F., & Faruque, M. R. I. (2020). Wide bandwidth angle-and polarization-insensitive symmetric metamaterial absorber for X and Ku band applications. *Scientific Reports*, *10*(1), 10338. doi: 10.1038/s41598-020-67262-5.

Hannan, S., Islam, M. T., Faruque, M. R. I., Chowdhury, M. E., & Musharavati, F. (2021). Angle-insensitive co-polarized metamaterial absorber based on equivalent circuit analysis for dual band WiFi applications. *Scientific reports*, *11*(1), 13791. doi: 10.1038/s41598-021-93322-5.

Hannan, S., Islam, M. T., Faruque, M. R. I., & Rmili, H. (2021). Polarization-independent perfect metamaterial absorber for C, X and, Ku band applications. *Journal of Materials Research and Technology*, *15*, 3722-3732. doi: 10.1016/j.jmrt.2021.10.007.

Hannan, S., Islam, M. T., Faruque, M. R. I., Chowdhury, M. E., & Musharavati, F. (2021). Angle-insensitive co-polarized metamaterial absorber based on equivalent circuit analysis for dual band WiFi applications. *Scientific reports*, *11*(1), 13791. doi: 10.1038/s41598-021-93322-5.

Hannan, S., Islam, M. T., Almalki, S. H., Faruque, M. R. I., & Islam, M. S. (2022). Rotational symmetry engineered, polarization and incident angle-insensitive, perfect metamaterial absorber for X and Ku band wireless applications. *Scientific Reports*, *12*(1), 3740. doi: 10.1038/s41598-022-07824-x.

Hannan, S., Islam, M. T., Soliman, M. S., Sahar, N. B. M., Singh, M. S. J., Faruque, M. R. I., & Alzamil, A. (2022). A filling-factor engineered, perfect metamaterial absorber for multiple applications at frequencies set by IEEE in C and X bands. *Journal of Materials Research and Technology*, *19*, 934-946. doi: 10.1016/j.jmrt.2022.05.071.

Haque, E., Hossain, M. A., Ahmed, F., & Namihira, Y. (2018). Surface plasmon resonance sensor based on modified $ D $-shaped photonic crystal fiber for wider range of refractive index detection. *IEEE Sensors Journal*, *18*(20), 8287-8293. doi: 10.1109/JSEN.2018.2865514.

Hasan, M. M., Faruque, M. R. I., & Islam, M. T. (2018). Dual band metamaterial antenna for LTE/bluetooth/WiMAX system. *Scientific reports*, *8*(1), 1240. doi: 10.1038/s41598-018-19705-3.

Hossain, I., Islam, M. T., Samsuzzaman, M., Moniruzzaman, M., Sahar, N. B. M., Almalki, S. H., ... Islam, M. S. (2022). Polarization insensitive split square ring resonator based epsilon-negative and near zero refractive index metamaterial for S, C, and X frequency bands satellite and radar communications. *Scientific Reports*, *12*(1), 9294. doi: 10.1038/s41598-022-12322-1.

Hossain, M. B., Faruque, M. R. I., Islam, M. T., Singh, M., & Jusoh, M. (2022). Triple band microwave metamaterial absorber based on double E-shaped symmetric split ring resonators for EMI shielding and stealth applications. *Journal of Materials Research and Technology*, *18*, 1653-1668. doi: 10.1016/j.jmrt.2022.03.079.

Hossain, M. B., Faruque, M. R. I., & Islam, M. T. (2023). Double elliptical resonator based quadruple band metamaterial absorber for EMI shielding applications in microwave regime. *Alexandria Engineering Journal*, *69*, 193-206. doi: 10.1016/j.aej.2023.01.035.

International Telecommunication Union [ITU]. (2019). *Assessment on use of spectrum in the 10-17 GHz band for the GSO fixed-satellite service in Region 1 S Series Fixed satellite service*, Geneva: ITU. Retrieved from http://www.itu.int/ITU-R/go/patents/en

Ioannides, N. (1998). Novel opto-electronic and plastic fibre sensors. Published Doctoral dissertation: University of North London, England.

Jahan, M. I., Faruque, M. R. I., & Hossain, M. B. (2023). An X-shaped triple split ring resonator-based metamaterial perfect absorber with quad-band incident and polarization angle insensitivity for C, X, and Ku band applications. *Journal of Magnetism and Magnetic Materials*, *580*, 170940. doi: https://doi.org/10.1016/j.jmmm.2023.170940.

Kapoor, A., Mishra, R., & Kumar, P. (2022). Frequency selective surfaces as spatial filters: Fundamentals, analysis and applications. *Alexandria Engineering Journal*, *61*(6), 4263-4293. doi: 10.1016/j.aej.2021.09.046.

Kim, G. (2023). Wave Propagation in Periodic Acoustic Metamaterials: From 1D To 3D. Published Doctoral dissertation: California Institute of Technology, USA.

Kim, M., Jung, K., Choi, Y., Hwang, S. S., & Hyun, J. K. (2022). Coupled Solid and Inverse Antenna Stacks Above Metal Ground as Metamaterial Perfect Electromagnetic Wave Absorbers with Extreme Subwavelength Thicknesses. *Advanced Optical Materials*, *10*(10), 2101672.

Landy, N. I., Sajuyigbe, S., Mock, J. J., Smith, D. R., & Padilla, W. J. (2008). Perfect metamaterial absorber. *Physical review letters*, *100*(20), 207402. doi: 10.1103/PhysRevLett.100.207402.

Lee, D., Hwang, J. G., Lim, D., Hara, T., & Lim, S. (2016). Incident angle- and polarization-insensitive metamaterial absorber using circular sectors. *Scientific reports*, *6*(1), 27155. doi: 10.1038/srep27155.

Moniruzzaman, M., Islam, M. T., Mansor, M. F., Soliman, M. S., Misran, N., & Samsuzzaman, M. (2023). Tuning metallic stub loaded symmetrical resonator based dual band metamaterial absorber for wave shielding from Wi-Fi frequencies. *Alexandria Engineering Journal*, *63*, 399-414. doi: 10.1016/j.aej.2022.07.051.

Norouzi, M., Jarchi, S., Ghaffari-Miab, M., Esfandiari, M., Lalbakhsh, A., Koziel, S., ... Moloudian, G. (2023). 3D metamaterial ultra-wideband absorber for curved surface. *Scientific Reports*, *13*(1), 1043. doi: 10.1038/s41598-023-28021-4.

Pang, H., Duan, Y., Huang, L., Song, L., Liu, J., Zhang, T., ... & Liu, X. (2021). Research advances in composition, structure and mechanisms of microwave absorbing materials. *Composites Part B: Engineering*, *224*, 109173. doi: https://doi.org/10.1016/j.compositesb.2021.109173.

Panwar, R., & Lee, J. R. (2017). Progress in frequency selective surface-based smart electromagnetic structures: A critical review. *Aerospace Science and Technology*, *66*, 216-234. doi: https://doi.org/10.1016/j.ast.2017.03.006.

Patel, S. K., Parmar, J., & Katkar, V. (2022). Ultra-broadband, wide-angle plus-shape slotted metamaterial solar absorber design with absorption forecasting using machine learning. *Scientific Reports*, *12*(1), 10166. doi: 10.1038/s41598-022-14509-y.

Ra'di, Y., Simovski, C. R., & Tretyakov, S. A. (2015). Thin perfect absorbers for electromagnetic waves: theory, design, and realizations. *Physical Review Applied*, *3*(3), 037001. doi: 10.1103/PhysRevApplied.3.037001.

Ramachandran, T., Faruque, M. R. I., Siddiky, A. M., & Islam, M. T. (2021). Reduction of 5G cellular network radiation in wireless mobile phone using an asymmetric square shaped passive metamaterial design. *Scientific Reports*, *11*(1), 2619. doi: 10.1038/s41598-021-82105-7.

Saadeldin, A. S., Sayed, A. M., Amr, A. M., Sayed, M. O., Hameed, M. F. O., & Obayya, S. S. A. (2023). Broadband polarization insensitive metamaterial absorber. *Optical and Quantum Electronics*, *55*(7), 652. doi: 10.1007/s11082-023-04881-y.

Sakib, S., Hoque, A., Rahim, S. K. B. A., Singh, M., Sahar, N. M., Islam, M. S., ... Islam, M. T. (2023). A central spiral split rectangular-shaped metamaterial absorber surrounded by polarization-insensitive ring resonator for S-band applications. *Materials*, *16*(3), 1172. doi: 10.3390/ma16031172.

Schultz, J. W. (2023). *Wideband Microwave Materials Characterization*. USA: Artech House.

Uddin, M. K., Hannan, S., Hossen, S., Gafur, A., Rashid, S. Z., Uddin, M. J., … Chowdhury, A. R., (2023). *Split-Ring Enclosed K-shaped Rotational Symmetric Metamaterial Absorber for Multiband Wireless Applications.* Paper presented at the 2023 International Conference on Next-Generation Computing, IoT and Machine Learning (NCIM) (pp. 1-6). IEEE. doi: 10.1109/NCIM59001.2023.10212969.

Ushikoshi, D., Higashiura, R., Tachi, K., Fathnan, A. A., Mahmood, S., Takeshita, H., ... Wakatsuchi, H. (2023). Pulse-driven self-reconfigurable meta-antennas. *Nature Communications*, *14*(1), 633. doi: 10.1038/s41467-023-36342-1.

Yufei, Z. H. A. N. G., Wenrong, Y. A. N. G., Xiaonan, L. I., & Guoqiang, L. I. U. (2023). Design and analysis of a broadband microwave

metamaterial absorber. *IEEE Photonics Journal*, 3, 1-10. doi: 10.1109/JPHOT.2023.3277449.

Zolfaghary pour, S., Chegini, E., & Mighani, M. (2023). Design of wideband metamaterial absorber using circuit theory for X-band applications. *IET Microwaves, Antennas & Propagation*, *17*(4), 292-300. doi: 10.1049/mia2.12338.